Single-/Few-Layer Graphene as Long-Lasting Electrocatalyst for Hydrogen Evolution Reaction

L. Najafi,[†,∥] S. Bellani,[†,∥] R. Oropesa-Nuñez,[‡] B. Martín-García,[†] M. Prato,[§] and F. Bonaccorso*[,†,‡]

[†]Graphene Labs, Istituto Italiano di Tecnologia, via Morego 30, 16163 Genova, Italy

[‡]BeDimensional Spa, Via Albisola 121, 16163 Genova, Italy

[§]Materials Characterization Facility, Istituto Italiano di Tecnologia, via Morego 30, 16163 Genova, Italy

ABSTRACT: The development of carbonaceous materials electrocatalytically active for water splitting reactions could overcome multiple disadvantages of metallic catalysts, including high cost, low selectivity, poor durability, and susceptibility to evolved gas. General guidelines to design carbon-based hydrogen evolution reaction (HER) electrocatalysts still remain a topic of debate. Here, we identify single-/few-layer graphene flakes with defective edges (SLG/FLG-DE), produced by hydrogen peroxide-assisted cosolvent liquid phase exfoliation, as durable and efficient HER electrocatalysts. The SLG/FLG-DE display overpotentials at 10 mA cm^{-2} of 55 and 85 mV in 0.5 M H_2SO_4 and 1 M KOH solutions, respectively, as well as a durable HER activity over 200 h.

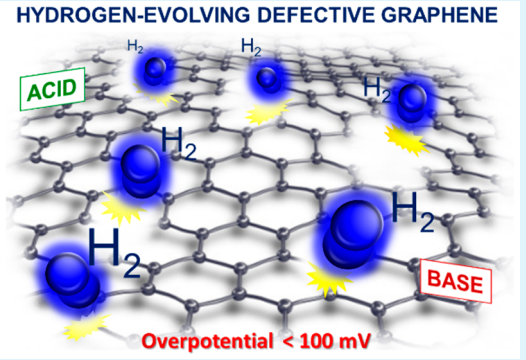

KEYWORDS: *graphene, electrocatalysts, hydrogen evolution reaction (HER), defects, liquid phase exfoliation*

Molecular hydrogen production through electrochemical water splitting represents a sustainable approach to produce a nonpolluting fuel from renewable energy sources. However, the competitiveness of water splitting technologies on the energy market is partially hampered by the use of the Pt-group metals as the most efficient catalysts, which entail severe costs and unfeasible scaling-up. Efficient electrocatalysts based on non-noble metals,[1] such as base metals (W, Ni, Mo, and Co) and metal sulfides, selenides, carbides, nitrides, phosphides, oxides, and (oxy)hydroxides, have been also demonstrated. However, their gradual oxidation, undesirable morphological and/or crystalline structure changes, uncontrolled dissolution or agglomeration, susceptibility to gas poisoning, and negative environmental effects hinder their long-term applications using air or aerated electrolyte.[2]

In this context, several carbon nanomaterials (CNs), especially carbon nanotubes and graphene, have been recently demonstrated to be efficient electrocatalysts for water splitting reactions,[2,3] namely, hydrogen evolution reaction (HER) and oxygen evolution reaction (OER), as well as oxygen reduction reaction (ORR).[4] Contrariwise to metal-based catalytic materials, CNs feature abundance and strong tolerance to acid/alkaline environments, which are pivotal for targeting cost-effective and durable electrocatalysts. Renowned works reported the need of a heteroatom (e.g., N, S, P, and B) doping of CNs to originate electrocatalytic activities.[3,5] In particular, major catalytic models claim that the difference between the electronegativity of doping atoms and neighboring carbons causes a local charge polarization which triggers the electrocatalytic activities.[6,7] However, general guidelines to design carbon-based water splitting electrocatalysts are still not defined. Moreover, further misunderstandings came up since undoped CNs have been reported as effective electrocatalysts.[8,9] These results have been recently supported by theoretical calculations, which showed that both graphene defects/edges[8,9] and curvature (*waved graphene*)[10] can exhibit Pt-analogous activity. For the particular case of HER, Figure 1 reports the density functional theory calculations of Gibbs free energy profiles for HER at pH = 0 for the graphene in its pristine and chemically doped forms, including curvature effects and edges/defects, as extrapolated from refs 6−8. These data show that the HER activity of the graphene is strongly affected by the curvature (e.g., wrinkles and ripples) of its basal plane (which is inevitable for *most of graphene*, due to thermal vibrations, edge/defect instabilities, and solvent trapping and/or interaction), as well as by the heteroatom dopants and edges/defects. Moreover, such electrocatalytic players can synergistically enhance the HER activity of graphene, as observed for concomitant dopants and topological defects.[7] Additionally, recent investigations have claimed that the origin of the electrocatalytic activity of graphene is ascribed to the presence of metallic impurities,[11] which are introduced by the synthetic procedures. Lastly, long-term (e.g., >10 h) durability of the electrocatalytic activity of graphene under continuous

Accepted: July 22, 2019

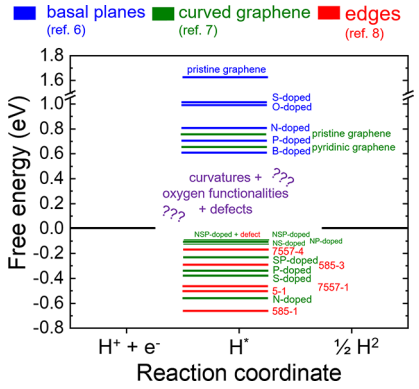

Figure 1. DFT calculations of Gibbs free energy profiles for HER at pH = 0 for graphene in its pristine and chemically doped basal planes, including curvature effects and edges/defects. H* indicates the adsorbed hydrogen. The data have been extrapolated from refs 6–8.

operation has not been established yet clearly through standard evaluation protocols. For the OER, anodic oxidation has been previously reported for carbon nanomaterials,[12] including graphite, graphene, and carbon nanotubes, especially in the presence of defective sites.[13] Therefore, caution should be warranted when dealing with such materials for ORR and OER.

In this work, we show that irregularly shaped and wrinkled single-/few-layer graphene flakes with defective edges (SLG/FLG-DE) hold striking activity for the water splitting reactions, although the durability of the electrocatalysts is exclusively proved for HER.

Experimentally, graphite powder was exfoliated into SLG/FLG-DE through a cosolvent-aided liquid phase exfoliation (LPE)[14] in *N*-methyl-2-pyrrolidone (NMP), as performed by adding a small amount of H_2O_2 (0.5 vol %) in the dispersion solvent (see the Supporting Information (SI), Experimental Section), followed by a thermal treatment at 1000 °C to

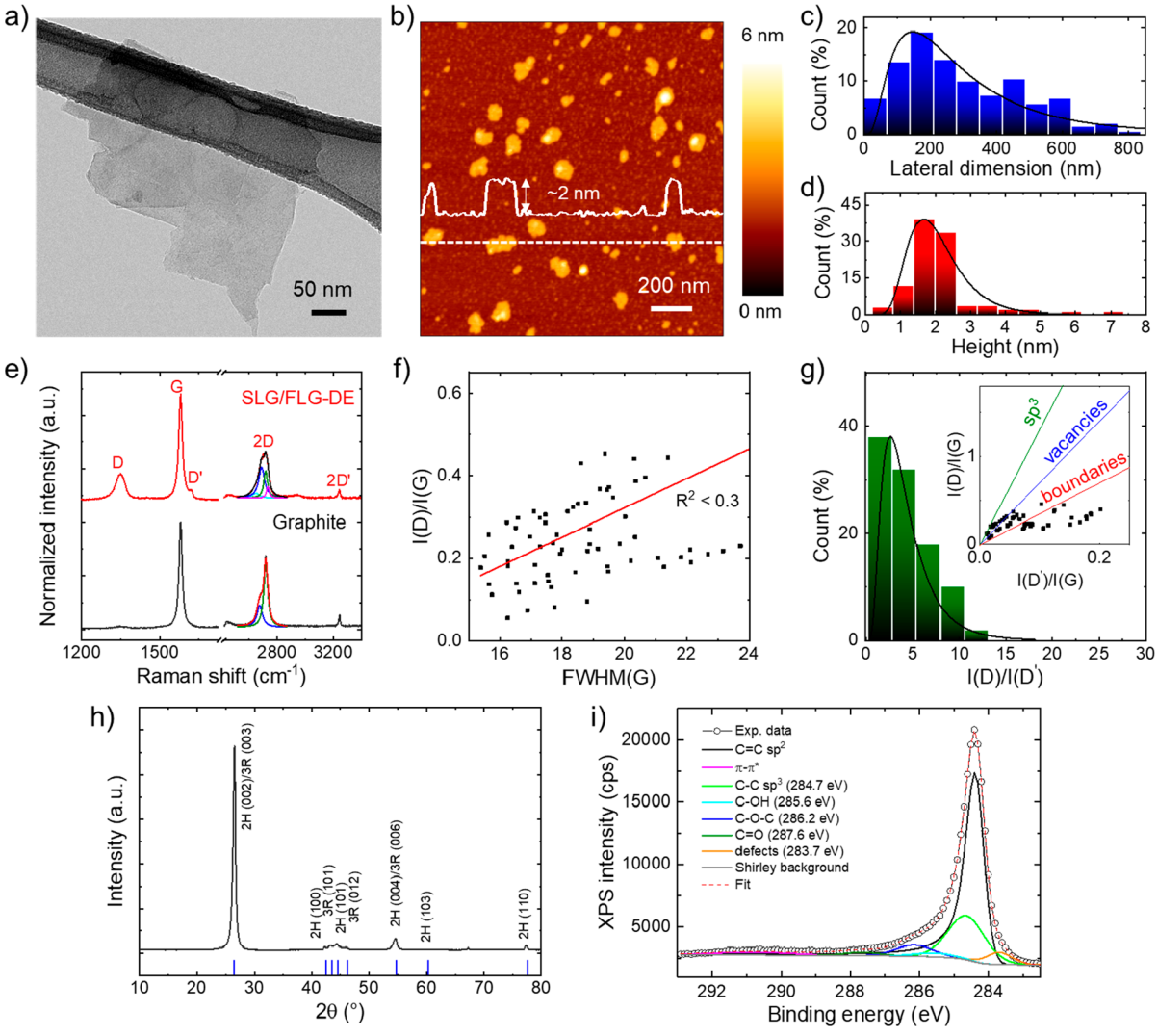

Figure 2. Morphological, structural, and chemical characterizations of the SLG/FLG-DE. (a) TEM and (b) AFM images of representative SLG/FLG-DE. (c) Lateral dimension and (d) thickness statistical analyses of SLG/FLG-DE (acquired on 80 flakes). (e) Comparison between the Raman spectra of the graphite and the SLG/FLG-DE. The multipeak Lorentzian fittings of the 2D mode Raman spectra show the contribution of the different 2D modes, i.e., $2D_1$ and $2D_2$, for the graphite and the four components for SLG/FLG-DE. (f) $I(D)/I(G)$ vs fwhm(G) plot for the SLG/FLG-DE. (g) Statistical analysis of $I(D)/I(D')$ for SLG/FLG-DE. The inset to panel g shows the $I(D)/I(G)$ vs $I(D')/I(G)$ plot. The colored straight lines indicate the conditions $I(D)/I(D') = 3.5$ (red), $I(D)/I(D') = 7$ (blue), and $I(D)/I(D') = 13$ (green), representing boundaries, vacancies, and sp^3 defects, respectively. (h) XRD spectra of SLG/FLG-DE. (i) C 1s XPS spectrum of SLG/FLG-DE and its deconvolution.

remove amorphous byproducts. In agreement with literature,[15] H_2O_2 promotes the exfoliation of graphite dispersed in NMP, also acting as an edge-selective oxidizing agent, without altering the crystallinity of the exfoliated flakes. In fact, the ultrasonication promotes the formation of reactive oxygen species (ROS) from H_2O_2 (and dissolved O_2), including hydroxyl radicals and singlet oxygen, which interact with the edges and grain boundaries of the graphitic planes, thus expanding and exfoliating the graphite. Moreover, ROS have been reported to foster the hydrogen abstraction on the methyl group of the NMP. This pathway takes place through the formation of an alkyl radical, which rearranges to formylpyrrolidone and *N*-hydroxymethylpyrrolidone, through a peroxy radical. Therefore, it is not excluded that such intermediate radical species and oxidative products can positively impact on the exfoliation of the graphite.

The lateral dimension and the thickness analyses of the exfoliated sample were carried out by transmission electron microscopy (TEM) (Figure 2a,c) and atomic force microscopy (AFM) (Figure 2b,d), respectively. The sample is composed of irregularly shaped wrinkled flakes with log-normal distribution of lateral dimension and thickness peaking at ∼147 and 1.7 nm, respectively. The measured thicknesses of the flakes indicate a massive presence of bilayer graphene, beyond single-layer graphene (SLG) and few-layer graphene (FLG). Noteworthy, the modified-LPE process results in flakes' thicknesses significantly inferior to those observed in samples produced by conventional LPE in NMP without H_2O_2 (SI Figure S1).

Raman spectroscopy measurements were performed to evaluate the structural quality of the exfoliated flakes, as well as to confirm their single-/few-layer-enriched composition. The typical Raman spectrum of exfoliated graphene flakes shows, as fingerprints, the G (E_{2g} phonon at the Brillouin zone center, ∼1585 cm^{-1}), the D (breathing mode of sp^2 rings requiring a defect for its activation by double resonance, ∼1380 cm^{-1}), the D′ (∼1620 cm^{-1}), and the 2D (∼2700 cm^{-1}) peaks (see SI for the detailed discussion of the origin of these Raman modes). Figure 2e shows the Raman spectra of the starting graphite and the exfoliated samples, normalized to the G peak. The Raman spectrum of the exfoliated sample exhibits an increase of the D peak compared to those of the native graphite. In particular, Raman statistical analysis (Figure S2) shows that the ratio between the intensities of the D and the G peaks—$I(D)/I(G)$—ranges between 0.1 and 0.6 for the exfoliated sample, whereas a negligible D peak is observed for the graphite. Previous studies on graphene have shown that D inevitably raises in graphene flakes, since intrinsic defects are located at their edges.[16] In the absence of a defective basal plane, $I(D)/I(G)$ varies inversely with the crystal size.[16] However, defects can also occur on the basal planes of the flakes (i.e., in the sp^2 carbon lattices). For such flakes, $I(D)/I(G)$ positively correlates with the amount of disorder.[16] In order to assess the crystal quality of the exfoliated flakes, the plot of $I(D)/I(G)$ vs fwhm(G) (fwhm = full width at half-maximum) can be used to identify the nature of the defects.[17] For our sample, the $I(D)/I(G)$ vs fwhm(G) plot (Figure 2f) does not show any linear correlation ($R^2 < 0.3$), which means that the H_2O_2-aided LPE process does not induce in-plane defects into the sample.[17] To further prove the nature of defects, the ratio between the intensities of the D and D′ peaks—$I(D)/I(D')$—can be experimentally analyzed.[18]

The statistical analysis of the $I(D)/I(D')$ (Figure 2g) shows values distributed between 1 and 13, evidencing the prevalence of a defective edge ($I(D)/I(D') \sim 3.5$ for boundaries; $I(D)/I(D') \sim 7$ for vacancies) and excluding defects associated with sp^3 hybridization (see also inset to Figure 2g).[18] The 2D band was analyzed to determine the thickness of the exfoliated flakes. Experimentally, graphite exhibits a 2D peak that results from two contributions, named $2D_1$ and $2D_2$. The intensity of $2D_2$ is around twice that of the $2D_1$.[19] Multilayer graphene (>5 layers) exhibits a 2D peak, which is almost identical, in terms of intensity and line shape, to the one of graphite.[16] Few-layer graphene, instead, has a $2D_1$ peak more intense than that of $2D_2$.[20] The 2D band splits into four peaks in bilayer graphene,[20] which is given by a single Lorentzian, corresponding to $2D_1$, in SLG.[20] As shown in Figure 2e, the 2D band of the exfoliated sample is deconvoluted in four peaks, thus indicating a large presence of bilayer graphene flakes, in agreement with the AFM characterization. The Raman analysis of the SLG/FLG produced by conventional LPE in NMP is reported in the SI (Figure S3), revealing a limited number of defective edges compared with SLG/FLG-DE.

The high crystallinity of SLF/FLG-DE was also confirmed by X-ray diffraction (XRD) measurements. In fact, their XRD pattern (Figure 2h) shows the (002) peak of the sp^2-hybridized graphitic structure at 26.5°, corresponding to an interlayer distance of 0.334 nm. The (002) peak position and the absence of XRD peaks at lower 2θ, corresponding to expanded graphitic structures, indicates that basal plane oxidation is negligible, and oxygen functionalities, evidenced hereinafter by X-ray photoelectron spectroscopy (XPS), are located onto the edges of the flakes. The other XRD peaks of graphite almost disappear as a consequence of the nanosizing of the starting graphite. The four peaks in the 2θ range of 40−49° show contributions of the (100) and (101) reflections of the hexagonal (2H) graphite and one of the (101) and (012) reflections of the rhombohedral (3R) symmetry phase,[21] indicating a deformation in the 2H structure of the graphite sheets observed in multilayered graphene flakes.[21]

X-ray photoelectron spectroscopy (XPS) measurements were performed to confirm the chemical and the structural properties of the exfoliated flakes discussed above. As shown in Figure 2i, the C 1s spectrum of the sample is dominated by a component peaking at 284.4 eV referring to C═C bonds (sp^2 carbon),[22] which also results in the corresponding feature at 290.8 eV ascribed to the to $\pi-\pi^*$ interactions.[22] The other components at 285.6, 286.2, and 287.6 eV are attributed to alcohol (C−OH), ether/epoxy (C−O−C), and ketone/aldehyde (C═O) functional groups on the surface, respectively. These components arise because defective edges of graphitic flakes are highly reactive toward adsorbing moisture, leading to the formation of oxygen functional groups.[23] Noteworthily, the data also show two more contributions peaking at 284.7 and 283.7 eV. The first one refers to the C−C bonds (sp^3 carbon)[24] or C adatoms[24,25] observed in the presence of defective edges (as well as to environmental contaminations, i.e., adventitious carbon). The second one has been recently ascribed to vacancy-like defects, which result in pentagon, heptagon, and octagons C rings.[24,25] The combination of the above spectroscopic characterizations points out that our exfoliated samples are mainly composed of graphitic flakes with single-/few-layer nature (morphological Raman analysis), and such flakes exhibit a high crystallinity in

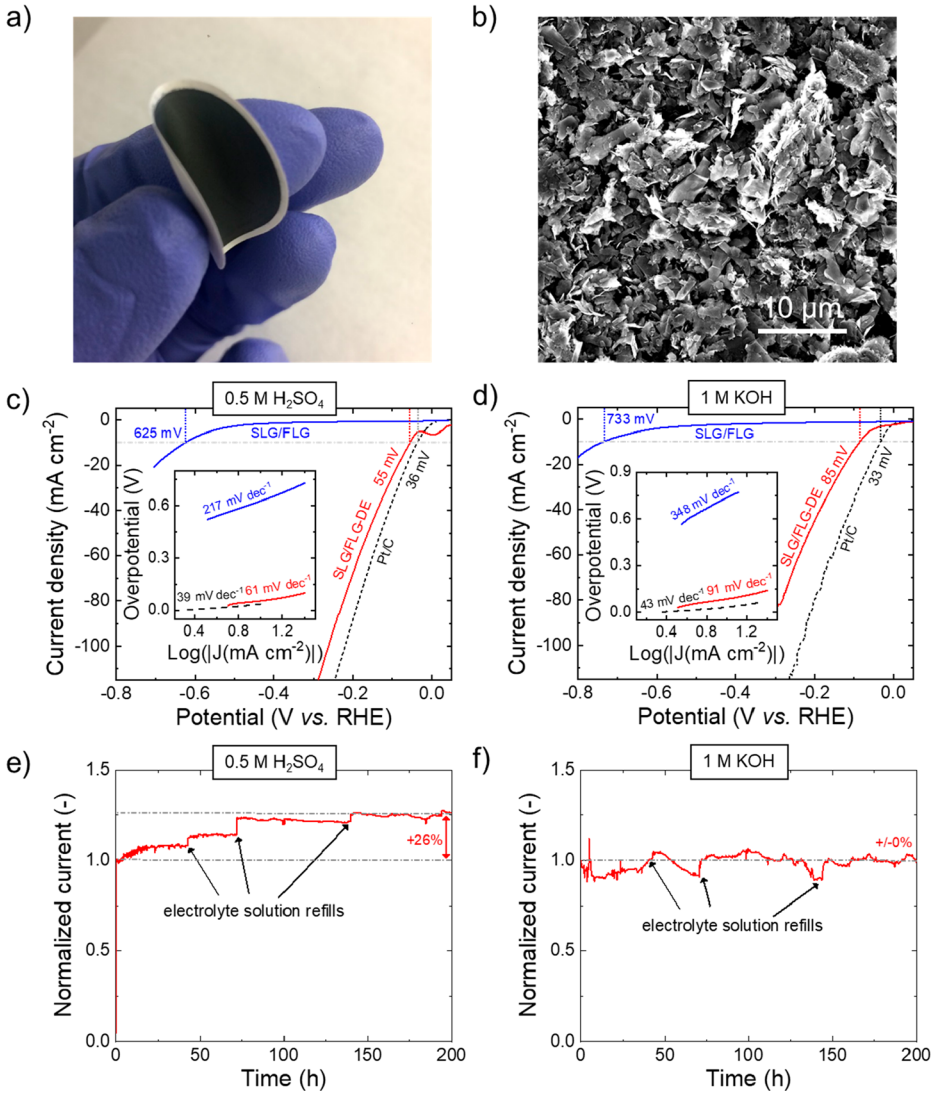

Figure 3. Morphological and electrochemical characterization for HER of the SLG/FLG-DE electrodes. (a) Photograph of a nylon filter-supported SLG/FLG electrode, illustrating its mechanical flexibility. (b) Top-view SEM image of a SLG/FLG-DE electrode. (c, d) *iR*-corrected cathodic LSV curves of the SLG/FLG-DE electrodes in acidic (0.5 M H_2SO_4) and alkaline (1 M KOH) solutions, respectively. The LSV curves of the SLG/FLG electrodes and Pt/C benchmarks are also shown for comparison. (e, f) Chronoamperometry measurements ($j-t$ curves) of the SLG/FLG-DE electrodes for HER in acidic (0.5 M H_2SO_4) and alkaline (1 M KOH) solution, respectively. Constant overpotentials were applied in order to give a starting cathodic current density of 80 mA cm^{-2}. The electrolyte solutions were refilled during the tests in order to compensate for the electrolyte losses caused by both the gas evolution and the water evaporation over time. Differently, the SLG/FLG electrodes show a Volmer step-limited HER activity, as expressed by their low Tafel slope values (217 and 348 mV dec^{-1} in 0.5 M H_2SO_4 and 1 M KOH, respectively). It is worth noticing that the HER kinetics of SLG/FLG-DE electrodes are faster than the ones mostly reported for metal-free HER electrocatalysts (see Supporting Information Table S1 and Table S2 for the HER performance in acidic and alkaline medium, respectively), and close to those of some non-noble metal-based benchmarks for HER.

their basal plane and abundant defective edges (XRD and XPS results).

The water splitting activity of SLG/FLG-DE was initially evaluated for HER in both acidic (0.5 M H_2SO_4) and alkaline (1 M KOH) N_2-purged solutions at room temperature. The electrodes were produced by depositing the SLG/FLG-DE dispersion onto a microporous nylon filter through a vacuum filtration process, in agreement with protocols previously reported for producing films of two-dimensional (2D) materials.[26−28] This process allows self-standing, flexible, and porous SLG/FLG-DE electrodes to be fabricated, excluding possible effects of the substrate on their electrochemical properties. Figure 3a shows a photograph of a representative SLG/FLG-DE electrode, evidencing its mechanical flexibility. The morphology of the as-prepared electrodes was analyzed by scanning electron microscopy (SEM). Figure 3b shows a top-view image of a representative SLG/FLG-DE electrode, whose surface has a crumpled, wrinkled flake-composed structure. Such structure is disordered with a random orientation of the flakes, some of them exposing their edges out of the substrate plane. Therefore, the defective edges are expected to actively participate to the water splitting reactions. Panels c and d of Figure 3 show the *iR*-corrected linear sweep voltammetry (LSV) curves for HER in 0.5 M H_2SO_4 and 1 M KOH, respectively, for the SLG/FLG-DE electrodes, compared to those measured for commercial Pt/C benchmarks and electrodes based on SLG/FLG produced by conventional LPE in NMP[14] (without H_2O_2 cosolvent). Surprisingly, the

SLG/FLG-DE electrodes show outstanding overpotentials at 10 mA cm^{-2} (η_{10}) as low as 55 and 85 mV in 0.5 M H_2SO_4 and 1 M KOH, respectively, not far from the η_{10} of the Pt/C benchmark (<40 mV). Noteworthily, the SLG/FLG electrodes display poor HER activities (η_{10} = 625 and 733 mV in 0.5 M H_2SO_4 and 1 M KOH, respectively), indicating that defective edges are crucial to promote the HER. In addition, such low HER activity of the SLG/FLG electrodes excludes the presence of HER-active metallic impurities, which could result from the starting graphite and are often considered the origin of the catalytic properties of CNs.[11] Importantly, the significant HER activity of SLG/FLG-DE electrodes is achieved without resorting to any electrochemical precondition treatment (e.g., electrochemical cycling). This also rules out the catalytic effects of the possible Pt contamination caused by the Pt counter-electrode dissolution and the redeposition of Pt atoms/clusters on the investigated electrodes during the electrochemical measurements. The correct evaluation of our SLG/FLG-DE electrodes was further confirmed by measuring their LSV curves for HER in 0.5 M H_2SO_4 and 1 M KOH by using a glassy carbon rod as the counter electrode (Figure S4). In fact, the LSV data show that the SLG/FLG-DE electrodes exhibit similar HER activities (e.g., almost identical η_{10}) among the different methods. Differently from the SLF/FLG electrodes, the SLG/FLG-DE electrodes exhibit a reduction peak at cathodic current densities lower than 10 mA cm^{-2}. This peak is tentatively attributed to a reduction of the defective edges of SLG/FLG-DE, which could be initially affected by the adsorption of environmental oxygen-based species (see XPS analysis). The Tafel slope is also a useful figure of merit to evaluate the HER kinetics at the electrocatalyst surface. Such a parameter is estimated from the linear portion of the Tafel plot (overpotential vs log(|current density|) curve) according to the Tafel equation (see the Experimental Section in the SI for further details). For an insufficient adsorbed hydrogen (H*) surface coverage, the Volmer reaction is the rate-limiting step of HER, and a theoretical Tafel slope of 120 mV dec^{-1} is expected. Conversely, in the limit of high H* surface coverage, the Tafel slope decreases toward theoretical values of 40/30 mV dec^{-1}, expressing the HER kinetics of the Heyrovsky/Tafel reactions. As shown by the inset to Figure 3c,d, the Tafel slopes obtained for the SLG/FLG-DE electrodes are 61 and 91 mV dec^{-1} in 0.5 M H_2SO_4 and 1 M KOH, respectively, suggesting that HER proceeds through a Volmer–Heyrovsky mechanism, in which hydrogen desorption is the rate-determining step.

Beyond the electrocatalytic activity, the durability is another important requirement of an electrocatalyst for practical applications. Panels e and f of Figure 3 show the long-term chronoamperometry measurements (j–t curves) for representative SLG/FLG-DE electrodes in 0.5 M H_2SO_4 and 1 M KOH, respectively. Constant overpotentials, providing a starting cathodic current density of 80 mA cm^{-2}, were applied over 200 h. Notably, the duration and the current densities adopted by our stability tests are considerably superior compared with those often applied to assess the stability of durable HER electrocatalysts ($\lesssim$30 mA cm^{-2} and $\lesssim$50 h, respectively). Our SLG/FLG-DE electrodes hold an excellent durability, showing an increase of the initial current density in 0.5 M H_2SO_4 (+26%) and an optimal current density retention in 1 M KOH. The origin of the fluctuations in the curves is caused by the electrolyte losses causes by gas evolution and water evaporation over several hours, as well as to the H_2 bubbling associated with cathodic current density higher than 80 mA cm^{-2}. The increase of the activity in acidic condition is attributed to favorable morphological changes of the SLG/FLG-DE electrodes during the HER (as shown by SEM analysis, Figure S5). In fact, the mechanical stresses originated by H_2 bubbling can cause a reorientation of the SLG/FLG-DE flakes, which progressively increase the H^+ accessibility to the HER-active sites of the electrodes. It is worth pointing out that the use of electrocatalyst binders, such as sulfonated tetrafluoroethylene-based fluoropolymer copolymers (e.g., Nafion), could prospectively "freeze" an optimized electrode morphology, preferably obtained during the deposition of the electrode films. Self-optimizing behavior of the SLG/FLG-DE electrodes could also be ascribed to the progressive cathodic reduction of the oxygen functionalities of the SLG/FLG-DE flakes (as suggested by the LSV data, Figure 3c), which are then activated for HER until the achievement of an electrochemical stability (after ~75 h). Notably, by simply soaking the SLG/FLG-DE electrodes in 0.5 M H_2SO_4 solution at their equilibrium potential (corresponding to a zero current density) over 100 h, no changes of the HER activities of the electrodes were observed. This is an advantage compared to affordable transition metal catalysts, such as Ni, which undergo a spontaneous dissolution in acidic electrolytes if sufficient cathodic potentials (typically <0.4 V vs RHE) are not applied.[29]

The electrocatalytic properties of the SLG/FLG-DE electrodes were further examined by OER experiments (Figure S6). Panels a and b of Figure S6 show the *iR*-corrected LSV curves of the SLG/FLG-DE electrodes for OER in 0.5 M H_2SO_4 and 1 M KOH, respectively, compared to those measured for commercial RuO_2 benchmarks and SLG/FLG electrodes. The SLG/FLG-DE electrodes display improved OER activities (η_{10} of 355 and 445 mV in 0.5 M H_2SO_4 and 1 M KOH, respectively) compared to those of the SLG/FLG electrodes (η_{10} of 618 and 1034 mV in 0.5 M H_2SO_4 and 1 M KOH, respectively). Consequently, an overall water splitting at 10 mA cm^{-2} can be attained with two SLG/FLG-DE electrodes at voltages as low as 1.641 and 1.712 V in 0.5 M H_2SO_4 and 1 M KOH, respectively (Figure S7). These values are consistent with the η_{10} measured for HER and OER for the SLG/FLG-DE electrodes in the corresponding solutions (see Figure 3c,d and Figure S5a,b, respectively). These results further exclude that the water splitting activities of the SLG/FLG-DE electrodes are originated by the possible metal contamination caused by the dissolution of the counter electrode, since the overall water splitting is measured in a symmetric two-electrode configuration with two identical SLG/FLG-DE electrodes. Despite the moderate OER activities of the SLG/FLG-DE electrodes, chronoamperometry measurements (Figure S6c,d) show a poor stability of the electrochemical performances (current density decreases of −57.7% and −66% in 0.5 M H_2SO_4 and 1 M KOH, respectively, after 3 h). The OER-activity degradation is attributed to the anodic oxidation of the SLG/FLG-DE electrodes toward gaseous products (e.g., CO_2 and CO), which causes a severe disruption of the electrodes visible by eye (Figure S8). The degrading behavior of the electrodes agrees with previous works,[13,30] which reported the electrochemical oxidation of graphitic materials (including graphite, graphene, and carbon nanotubes) under anodic potentials (e.g., >1.2 V vs RHE) in either acidic or alkaline solutions,[30] especially in the presence of defective

sites.[13] Therefore, our SLG/FLG-DE electrodes are currently recommended only for HER.

To summarize, irregularly shaped and wrinkled single-/few-layer graphene flakes with defective edges, above named as SLG/FLG-DE, are identified as efficient and highly durable electrocatalysts for HER. In particular, as-produced metal-free, and self-standing SLG-FLG-DE electrodes exhibit remarkable η_{10} of 55 and 85 mV in acidic (0.5 M H_2SO_4) and alkaline (1 M KOH) solutions, together with durable HER activities over 200 h of continuous operation. Such results point out the possibility to produce high-performance graphene-based HER electrocatalysts by envisioning their structural properties (without resorting to molecular design via complex synthetic and chemical functionalization strategies) and adopting scalable material production methods (e.g., LPE). It is important to notice that the origin of the catalytic activity of electrocatalysts based on CNs, including graphene, is currently the subject of strong debate. In fact, literature published in renowned journals claimed that both heteroatom (e.g., N, S, P, or B) doping[3,5−7] and defects[8,9] of CNs can originate Pt-analogous electrocatalytic activities, while other recent investigations reported that the electrocatalytic activity of CNs (especially graphene) is exclusively ascribed to metallic impurities/contaminations introduced by synthetic procedures.[11] In our case, the electrochemical characterization of single-/few-layer graphene flakes (named SLG/FLG), as obtained by prototypical LPE of the same native graphite used for the production of SLG/FLG-DE, revealed poor HER activity. This observation unambiguously indicates the need for defects to endow graphene-based electrodes with HER activity. Although we have correlated the defects to the HER activity of graphene flakes, it is not possible to rule out that the defects strongly trap a minimal amount (on the order of a few parts per million) of metallic impurities (including Fe, Ni, and Co, etc.),[11] which can locally alter the catalyst electronic structures to enhance the HER activity compared to either pristine graphene or metals. Moreover, although a large amount of literature on CN-based electrocatalyst focused on ORR and OER, our electrochemical characterizations warn against anodic oxidation phenomena, which cause the degradation of the OER activity of defective graphitic sites. Indeed, despite the bifunctional activities of the SLG/FLG-DE electrodes (η_{10} for OER of 355 and 445 mV in 0.5 M H_2SO_4 and 1 M KOH, respectively), we currently recommend their use only for HER. Overall, we believe that our results prove an experimentally scalable method to produce metal-free electrocatalyst for the water splitting reactions based on graphene flakes, triggering the scientific community to think seriously about the prompt exploitation of available graphene for electrochemical water splitting.

■ ASSOCIATED CONTENT

Supporting Information

The Supporting Information is available free of charge on the ACS Publications website at DOI: 10.1021/acsaem.9b00949.

TEM and AFM analyses; Raman statistical analyses and spectrum; LSV curves; SEM analysis; comparison between the HER performance of metal-free electrocatalysts (PDF)

■ AUTHOR INFORMATION

Corresponding Author

*Tel.: +39 01071781795. E-mail: francesco.bonaccorso@iit.it.

ORCID

M. Prato: 0000-0002-2188-8059

F. Bonaccorso: 0000-0001-7238-9420

Author Contributions

‖L.N. and S.B. contributed equally to this work.

Funding

This project has received funding from the European Union's Horizon 2020 research and innovation program under grant agreement no785219.-GrapheneCore2.

Notes

The authors declare no competing financial interest.

■ ACKNOWLEDGMENTS

We thank Sergio Marras (Materials Characterization Facility, Istituto Italiano di Tecnologia) for support in XRD data acquisition and analysis; Alberto Ansaldo (Graphene Labs, Istituto Italiano di Tecnologia) for support in thermal material treatment; the Electron Microscopy Facility, Istituto Italiano di Tecnologia for support in TEM data acquisition; and Andrea Toma for the access to the Clean Room facility, Istituto Italiano di Tecnologia for the SEM measurements.

■ ABBREVIATIONS

AFM = atomic force microscopy
HER = hydrogen evolution reaction
OER = oxygen evolution reaction
LPE = liquid phase exfoliation
LSV = linear scan voltammetry
NMP = *N*-methyl-2-pyrrolidone
ROS = reactive oxygen species
SBS = sedimentation-based separation
SEM = scanning electron microscopy
SLG/FLG = single-/few-layer graphene flakes
SLG/FLG-DE = single-/few-layer graphene flakes with defective edges
TEM = transmission electron microscopy
η_{10} = overpotential at 10 mA cm^{-2}.

■ REFERENCES

(1) Roger, I.; Shipman, M. A.; Symes, M. D. Earth-Abundant Catalysts for Electrochemical and Photoelectrochemical Water Splitting. *Nat. Rev. Chem.* **2017**, *1*, No. 0003.

(2) Liu, X.; Dai, L. Carbon-Based Metal-Free Catalysts. *Nat. Rev. Mater.* **2016**, *1*, 16064.

(3) Zhou, W.; Jia, J.; Lu, J.; Yang, L.; Hou, D.; Li, G.; Chen, S. Recent Developments of Carbon-Based Electrocatalysts for Hydrogen Evolution Reaction. *Nano Energy* **2016**, *28*, 29−43.

(4) Li, Y.; Zhou, W.; Wang, H.; Xie, L.; Liang, Y.; Wei, F.; Idrobo, J.-C.; Pennycook, S. J.; Dai, H. An Oxygen Reduction Electrocatalyst Based on Carbon Nanotube−graphene Complexes. *Nat. Nanotechnol.* **2012**, *7*, 394.

(5) Zheng, Y.; Jiao, Y.; Li, L. H.; Xing, T.; Chen, Y.; Jaroniec, M.; Qiao, S. Z. Toward Design of Synergistically Active Carbon-Based Catalysts for Electrocatalytic Hydrogen Evolution. *ACS Nano* **2014**, *8*, 5290−5296.

(6) Jiao, Y.; Zheng, Y.; Davey, K.; Qiao, S. Z. Activity Origin and Catalyst Design Principles for Electrocatalytic Hydrogen Evolution on Heteroatom-Doped Graphene. *Nat. Energy* **2016**, *1*, 16130.

(7) Ito, Y.; Shen, Y.; Hojo, D.; Itagaki, Y.; Fujita, T.; Chen, L.; Aida, T.; Tang, Z.; Adschiri, T.; Chen, M. Correlation between Chemical

Dopants and Topological Defects in Catalytically Active Nanoporous Graphene. *Adv. Mater.* **2016**, *28*, 10644−10651.
(8) Jia, Y.; Zhang, L.; Du, A.; Gao, G.; Chen, J.; Yan, X.; Brown, C. L.; Yao, X. Defect Graphene as a Trifunctional Catalyst for Electrochemical Reactions. *Adv. Mater.* **2016**, *28*, 9532−9538.
(9) Jiang, Y.; Yang, L.; Sun, T.; Zhao, J.; Lyu, Z.; Zhuo, O.; Wang, X.; Wu, Q.; Ma, J.; Hu, Z. Significant Contribution of Intrinsic Carbon Defects to Oxygen Reduction Activity. *ACS Catal.* **2015**, *5*, 6707−6712.
(10) Qu, Y.; Ke, Y.; Shao, Y.; Chen, W.; Kwok, C. T.; Shi, X.; Pan, H. Effect of Curvature on the Hydrogen Evolution Reaction of Graphene. *J. Phys. Chem. C* **2018**, *122*, 25331−25338.
(11) Mazánek, V.; Luxa, J.; Matějková, S.; Kučera, J.; Sedmidubský, D.; Pumera, M.; Sofer, Z. Ultrapure Graphene Is a Poor Electrocatalyst: Definitive Proof of the Key Role of Metallic Impurities in Graphene-Based Electrocatalysis. *ACS Nano* **2019**, *13*, 1574−1582.
(12) Kinoshita, K. *Carbon-Electrochemical and Physicochemical Properties*; John Wiley & Sons: Hoboken, NJ, USA, 1988.
(13) Dumitrescu, I.; Unwin, P. R.; Macpherson, J. V. Electrochemistry at Carbon Nanotubes: Perspective and Issues. *Chem. Commun.* **2009**, No. 45, 6886−6901.
(14) Bonaccorso, F.; Bartolotta, A.; Coleman, J. N.; Backes, C. 2D-crystals-based functional inks. *Adv. Mater.* **2016**, *28*, 6136−6166.
(15) Vittore, A.; Acocella, M. R.; Guerra, G. Edge-Oxidation of Graphites by Hydrogen Peroxide. *Langmuir* **2019**, *35*, 2244−2250.
(16) Lucchese, M. M.; Stavale, F.; Ferreira, E. H. M.; Vilani, C.; Moutinho, M. V. O.; Capaz, R. B.; Achete, C. A.; Jorio, A. Quantifying Ion-Induced Defects and Raman Relaxation Length in Graphene. *Carbon* **2010**, *48*, 1592−1597.
(17) Bracamonte, M. V.; Lacconi, G. I.; Urreta, S. E.; Foa Torres, L. E. F. On the Nature of Defects in Liquid-Phase Exfoliated Graphene. *J. Phys. Chem. C* **2014**, *118*, 15455−15459.
(18) Eckmann, A.; Felten, A.; Mishchenko, A.; Britnell, L.; Krupke, R.; Novoselov, K. S.; Casiraghi, C. Probing the Nature of Defects in Graphene by Raman Spectroscopy. *Nano Lett.* **2012**, *12*, 3925−3930.
(19) Ferrari, A. C.; Basko, D. M. Raman Spectroscopy as a Versatile Tool for Studying the Properties of Graphene. *Nat. Nanotechnol.* **2013**, *8*, 235.
(20) Cançado, L. G.; Reina, A.; Kong, J.; Dresselhaus, M. S. Geometrical Approach for the Study of G′ Band in the Raman Spectrum of Monolayer Graphene, Bilayer Graphene, and Bulk Graphite. *Phys. Rev. B: Condens. Matter Mater. Phys.* **2008**, *77*, 245408.
(21) Seehra, M. S.; Geddam, U. K.; Schwegler-Berry, D.; Stefaniak, A. B. Detection and Quantification of 2H and 3R Phases in Commercial Graphene-Based Materials. *Carbon* **2015**, *95*, 818−823.
(22) Siokou, A.; Ravani, F.; Karakalos, S.; Frank, O.; Kalbac, M.; Galiotis, C. Surface Refinement and Electronic Properties of Graphene Layers Grown on Copper Substrate: An XPS, UPS and EELS Study. *Appl. Surf. Sci.* **2011**, *257*, 9785−9790.
(23) Liu, Z.; Zhao, Z.; Wang, Y.; Dou, S.; Yan, D.; Liu, D.; Xia, Z.; Wang, S. In Situ Exfoliated, Edge-Rich, Oxygen-Functionalized Graphene from Carbon Fibers for Oxygen Electrocatalysis. *Adv. Mater.* **2017**, *29*, 1606207.
(24) Barinov, A.; Malcioğlu, O. B.; Fabris, S.; Sun, T.; Gregoratti, L.; Dalmiglio, M.; Kiskinova, M. Initial Stages of Oxidation on Graphitic Surfaces: Photoemission Study and Density Functional Theory Calculations. *J. Phys. Chem. C* **2009**, *113*, 9009−9013.
(25) Yamada, Y.; Yasuda, H.; Murota, K.; Nakamura, M.; Sodesawa, T.; Sato, S. Analysis of Heat-Treated Graphite Oxide by X-Ray Photoelectron Spectroscopy. *J. Mater. Sci.* **2013**, *48*, 8171−8198.
(26) Najafi, L.; Bellani, S.; Oropesa-Nuñez, R.; Ansaldo, A.; Prato, M.; Del Rio Castillo, A.; Bonaccorso, F. Engineered $MoSe_2$-Based Heterostructures for Efficient Electrochemical Hydrogen Evolution Reaction. *Adv. Energy Mater.* **2018**, *8*, 1703212.
(27) Najafi, L.; Bellani, S.; Oropesa-Nuñez, R.; Ansaldo, A.; Prato, M.; Del Rio Castillo, A. E.; Bonaccorso, F. Doped-$MoSe_2$ Nanoflakes/3d Metal Oxide−Hydr(Oxy)Oxides Hybrid Catalysts for PH-Universal Electrochemical Hydrogen Evolution Reaction. *Adv. Energy Mater.* **2018**, *8*, 1801764.
(28) Petroni, E.; Lago, E.; Bellani, S.; Boukhvalov, D. W.; Politano, A.; Gürbulak, B.; Duman, S.; Prato, M.; Gentiluomo, S.; Oropesa-Nuñez, R.; Panda, J. K.; Toth, P. S.; Del Rio Castillo, A. E.; Pellegrini, V.; Bonaccorso, F. Liquid-Phase Exfoliated Indium−Selenide Flakes and Their Application in Hydrogen Evolution Reaction. *Small* **2018**, *14*, 1800749.
(29) Lu, J.; Xiong, T.; Zhou, W.; Yang, L.; Tang, Z.; Chen, S. Metal Nickel Foam as an Efficient and Stable Electrode for Hydrogen Evolution Reaction in Acidic Electrolyte under Reasonable Overpotentials. *ACS Appl. Mater. Interfaces* **2016**, *8*, 5065−5069.
(30) Yi, Y.; Weinberg, G.; Prenzel, M.; Greiner, M.; Heumann, S.; Becker, S.; Schlögl, R. Electrochemical Corrosion of a Glassy Carbon Electrode. *Catal. Today* **2017**, *295*, 32−40.

NOTE ADDED AFTER ASAP PUBLICATION

This paper was published on the Web on July 29, 2019, with the wrong Supporting Information file. The correct Supporting Information was uploaded, and the corrected version was reposted on July 31, 2019.